Analysis of acoustic emission signals during fatigue testing of a M36 bolt using the Hilbert-Huang spectrum

Félix Leaman[*1], Aljoscha Herz[1], Victoria Brinnel[2],
Ralph Baltes[1] and Elisabeth Clausen[1]

[1]Institute for Advanced Mining Technologies, RWTH Aachen University, Germany
[2] Institute for Ferrous Metallurgy, RWTH Aachen University, Germany

Abstract. One of the most important aspects in structural health monitoring is the detection of fatigue damage. Structural components such as heavy-duty bolts work under high dynamic loads, and thus are prone to accumulate fatigue damage and cracks may originate. Those heavy-duty bolts are used, for example, in wind power generation and mining equipment. Therefore, the investigation of new and more effective monitoring technologies attracts a great interest. In this study the acoustic emission (AE) technology was employed to detect incipient damage during fatigue testing of a M36 bolt. Initial results showed that the AE signals have a high level of background noise due to how the load is applied by the fatigue testing machine. Thus, an advanced signal processing method in the time-frequency domain, the Hilbert-Huang Spectrum (HHS), was applied to reveal AE components buried in background noise in form of high-frequency peaks that can be associated with damage progression. Accordingly, the main contribution of the present study is providing insights regarding the detection of incipient damage during fatigue testing using AE signals and providing recommendations for further research.

Keywords: acoustic emission; empirical mode decomposition; Hilbert-Huang spectrum; crack detection; structural health monitoring

1. Introduction

Heavy-duty steel bolts are widely used to support structures in offshore wind turbines, in the mining industry and in a variety of steel constructions. In such applications, high loads and variable operating frequencies in service are usual. Therefore, an accumulation of fatigue damage can occur and cracks can develop. Currently, the knowledge about crack initiation and propagation in such large bolts is limited. Recent studies on the failure properties of such bolts revealed that the crack growth concentrates on the thread (Stranghöner *et al*. 2018). The studies proved that a conservative design of such bolts is possible, but for a real understanding of the fatigue and failure behavior the application of modern simulations and measurement methods is required. While simulation methods for damage mechanics are available, the experimental observation of crack initiation and growth is more challenging in such bolts. The use of potential drop techniques is, for example, hindered by

---

the fact that the crack sometimes initiates beneath the zinc coating and by the complex geometry of a bolted connection. Yet, determining the initial crack and crack propagation monitoring is essential for a real understanding of the failure of such structures, as well as for efficient testing in time-consuming fatigue experiments.

Among structural health monitoring systems, technologies based on piezoelectric transducers have been extensively used as a non-destructive technique for damage detection (Li *et al*. 2014). Within these technologies, the acoustic emission (AE) technology employs passive sensors sensitive to elastic wave propagation in solids. Normally, the AE signals consist of a continuous emission component with random nature and transient AE bursts coming from specific sources (Ono *et al*. 2005). Huang M *et al*. (1998) indicated that most AE sources in materials are damage-related, like crack initiation and growth, crack opening and closure and dislocation movement, among others. During fatigue testing different sources such as impacts, friction and damage propagation can generate AE signals. Thus, signal processing techniques must be used to filter out unwanted components. Crack initiation is determined by the first appearance of the AE signals at low stress levels. Also former works from Han *et al*. (2011), Keshtgar *et al*. (2013), Nair *et al*. (2014), Kratochvilova *et al*. (2017) and Du and Li (2019) showed a good correlation for damage severity, crack growth and crack length to AE features such as amplitude, duration, count rate, energy and others. More recent research has brought new insights regarding the relationship between AE events measured during fatigue tests (Danyuk *et al*. 2017, Bhuiyan *et al*. 2018).

Due to the non-stationary and non-linear characteristics of the AE signals, conventional analysis tools used for example in vibration analysis, must be carefully used. Moreover, in heavy-duty structures subjected to high dynamic loads, it is usual to have other sources of AE that are not damage-related. Some of these sources are friction and impacts (Vraetz *et al*. 2016). These effects could mask AE signals related to damage, especially at early stages (Carlos 2003). Nevertheless, in recent years advanced signal processing techniques such as wavelet transform, spectral kurtosis or Hilbert-Huang spectrum (HHS) have been applied to face these problems (Yang *et al.* 2014, Ruiz-Carcel *et al.* 2014, Zhao *et al*. 2019). In this work, the use of the HHS which is based on the empirical mode decomposition (EMD) is investigated. The EMD is an algorithm that adaptively decomposes a signal into several intrinsic mode functions (IMFs). These IMFs have characteristics that allow a well-behaved Hilbert transform (Huang N *et al*. 1998). Thus, the analysis of the instantaneous frequency of the signal makes sense. Based on this, the HHS is a representation of the signal´s instantaneous frequency and instantaneous amplitude over time.

Several authors have applied the EMD and HHS to the analysis of AE signals. Zhang *et al*. (2017) used the EMD for noise cancellation in AE signals from a rail-wheel test rig. First, an AE signal coming from a crack was measured as reference signal. The main frequency of this signal was 150 kHz. The reference signal was used together with a cross-correlation analysis to select which IMFs contains useful information. Then, wavelet analysis was used to detect AE crack signals in further tests under operation. WenQin *et al*. (2016) indicated that the HHS of AE signals can clearly illustrate the frequency content of IMF components in different damage stages during tensile tests. Lu *et al*. (2011) carried out a comparative study of STFT, wavelet transform and HHS for the analysis of AE signals during a tensile test of a carbon fiber reinforced plastic. They concluded that the HHS had better performance in dealing with these no-stationary AE signals and that the frequencies in the IMF components can reveal different damage modes. Siracusano *et al*. (2016) formulated a framework based on the HHS to discriminate between cracking modes in a concrete specimen. Hamdi *et al*. (2013) used the HHS to perform classification of damage mechanisms of polymer-composite materials. Their analysis showed that the frequency content of the IMFs can provide

information about the damage mechanisms. In the following, the HHS is used as a tool to analyze AE signals from a M36 steel bolt during a fatigue test.

2. Description of the methods

The HHS is a time-frequency signal processing technique suited for the analysis of AE signals (Huang N *et al*. 1998). The key part to construct the HHS is the EMD algorithm, which adaptively decomposes a signal into several IMFs. These IMFs reflect local characteristics of the signal in time-scale. After the IMFs are obtained, the Hilbert transform (HT) is applied to each of them and the instantaneous frequency and amplitude are calculated. Finally, the HHS of each IMF consists of a 3d-plot of time, instantaneous frequency and instantaneous amplitude, in which the energy-frequency structure of a signal can be evaluated over time.

2.1 Empirical mode decomposition

Let $x(t)$ be the signal under analysis. The IMFs of $x(t)$ are obtained iteratively using the following sifting algorithm. First, all the local extrema of $x(t)$ are detected and connected with cubic splines (maxima and minima, separately). This generates two envelopes signals: the upper envelope $u_1(t)$ and the lower envelope $v_1(t)$. Then, a mean envelope $m_1(t)$ is calculated by taking the average of the other two envelopes as shown in Eq. (1).

$$m_1(t) = \frac{u_1(t) + v_1(t)}{2} \tag{1}$$

Then, the mean envelope $m_1(t)$ is subtracted from the signal $x(t)$ and a signal $h_{11}(t)$ is obtained as shown in Eq. (2).

$$h_{11}(t) = x(t) - m_1(t) \tag{2}$$

This process is repeated several times using the signal $h_{1k}(t)$ obtained in the iteration k as input signal for the iteration $k+1$. When a stopping criterion is achieved in the iteration n, the signal $h_{1n}(t)$ is designated $c_1(t)$ as the first IMF from $x(t)$. The difference between the signal $x(t)$ and $c_1(t)$ is called the residual $r_1(t)$. To obtain the second IMF the sifting algorithm must be applied to this residual $r_1(t)$. Therefore, to obtain the IMF $c_{i+1}(t)$ the sifting algorithm must be applied to the residual $r_i(t)$. The residual is no longer useful, i.e. no more meaningful IMFs can be obtained from it, when it is only a sine wave or contains no more oscillations.

The original stoppage criteria proposed by Huang N *et al*. (1998) for the sifting algorithm is based on the standard deviation between two consecutive results from iterations of the sifting algorithm. This criterion is defined in Eq. (3). Typical values for the tolerance are between 0.2 and 0.3.

$$\sum_t \left[\frac{h_k(t) - h_{k-1}(t)}{h_{k-1}(t)} \right]^2 < tol. \tag{3}$$

2.2 Hilbert-Huang spectrum

The HT is applied to each IMF $c_i(t)$ to obtain the respective analytical signal $c_{i,a}(t)$ as shown in

Eq. (4).

$$c_{i,a}(t) = c_i(t) + jH[c_i(t)] \tag{4}$$

In Eq. (4) j is the imaginary unit and H[•] is the HT operator. Using the analytical signal the instantaneous amplitude $a(t)$ is obtained by taking the magnitude of the complex values and the instantaneous phase $\theta(t)$ by calculating the angle. Then, the phase must be unwrapped and the instantaneous frequency $\omega(t)$ can be calculated using Eq. (5).

$$\omega(t) = \frac{d\theta(t)}{dt} \tag{5}$$

Finally, the HHS is constructed by using the time t in the x-axis, the instantaneous frequency $\omega(t)$ in the y-axis, and the instantaneous amplitude $a(t)$ in the z-axis (or representative color-map). Thus, the HHS is a frequency-time distribution of each IMF.

3. Experimental procedure

The specimen was a M36x295 HV 10.9 high strength steel bolt. Fatigue testing was performed in order to induce a defined pre-crack. The thread of the bolt was notched using a cutter, leading to a decrease of loading cycles and to ensure the technical crack initiation spot. After fatigue testing, the bolt was led to fracture in a final tensile test in order to analyze the fracture surface without performing a complete fatigue test and thus time-consuming experiment. A servo-hydraulic testing machine with a maximum force of 1000 kN was used to perform the experiment. The specimen was tested under two different load conditions (LCs) illustrated in Table 1. The average load throughout the whole test was 500 kN using different upper and lower loads. The oscillating frequency was constant with 7 Hz. The upper and lower loads for the LC N°1 were 550 and 450 kN, respectively. After approximately 25.200 loading cycles, the upper and lower loads were changed to 600 and 400 kN (LC N°2). The test proceeded until approximately 30240 loading cycles were completed (25200 for LC N°1 and 5040 for LC N°2). The purpose of the LC N°1 was to initiate the fatigue pre-crack at the machined notch. During the LC N°2 the crack was supposed to grow. Crack growth mainly happened around the thread.

The AE data acquisition system consisted of a NI-9223 measurement card with a sampling frequency of 1 MHz. Because of the different mounting spaces available between bolt and machine at both ends of the bolt, different AE sensors must be used. A threaded AE sensor VS 370-A was mounted on top of the bolt (near the notch) and one AE sensor was VS 375-M mounted at the bottom

Table 1 Conditions of the test

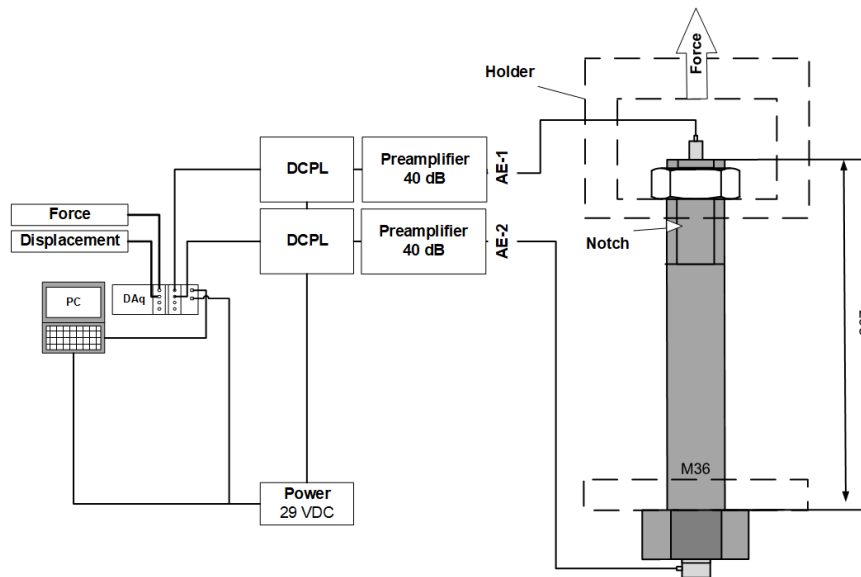| Parameter	LC N°1	LC N°2
F_{upper} [kN]	550	600
F_{lower} [kN]	450	400
Duration [min]	60	12
Cycles	25200	5040
Tensile test	Until failure	

Fig. 1 Test setup for AE data acquisition

(see Fig. 1). Both sensors can be considered broadband sensors with frequency ranges from 170 to 590 kHz and from 250 to 750 kHz, and peak frequencies of 370 and 375 kHz, respectively. The signals were pre-amplified with 40 dB. Both sensors were mounted using magnetic holders and copper paste was used to enhance the acoustic coupling. In order to perform the tensile test on the bolt, a special magnetic holder was needed for the sensor at the top. As indicated in Fig. 1, the lock nut as well as the bolt head had direct contact to the holder.

4. Results

4.1 Inspection of the specimen after tensile test

Fig. 2 shows the final fracture surface of the specimen after the tensile test. The fatigue pre-crack on the outer region of the thread can be clearly recognized by its light grey color. The dark grey area in the center of the specimen represents the ductile fracture surface of the final fracture in the tensile test. The fatigue crack region is highlighted by two shades of light grey, separated by the line of rest induced by the change of the LC. Consequently, the fatigue crack was introduced during the LC N°1 and progressed in the LC N°2.

4.2 Comparison of both load conditions

Two AE signals were chosen to illustrate the results. The first signal was taken from the beginning of the LC N°1 (around cycle N°2700), while the second from the end of LC N°2 (around cycle N°4000). Fig. 3 shows the AE signals for the channels AE-1 and AE-2 considering both LCs. Instead of a series of transient bursts over a continuous noise, in the figures waveforms with modulated amplitude are present. In the signals with duration of 1.048 s a total of 15 amplitude
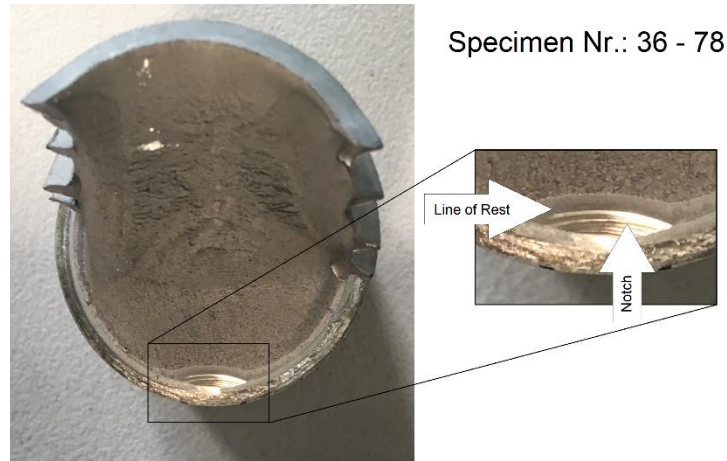
Fig. 2 Specimen after the tensile test

peaks are shown, which correspond to the maximal and minimal traction points of the load with frequency of 7 Hz. Due to the appearance of the AE signals, it is impossible to distinguish transient AE bursts. The use of filtering (highpass, lowpass or bandpass) did not improve the detection of AE bursts. For the channel AE-1 it is also observable, that an increment of 50 kN in the traction force produces an increase of the AE amplitude from 100 to 300 mV when the specimen is under maximal traction. On the other hand, small influence is observable when the specimen is under minimal traction. In this case a decrement of 50 kN in the traction force produces negligible changes in the AE amplitude, which for both LCs is approximately 100 mV. The same behavior is observable for channel AE-2, but with higher amplitudes.

The EMD for both signals was carried out using a tolerance of 0.2 for the sifting algorithm according to Eq. (3). Due to the high frequency and stochastic nature of the AE (Ono *et al.* 2005), rapid and high frequency variations were found in the instantaneous frequencies, making the analysis of the HHS difficult. To avoid this, the instantaneous frequencies $\omega(t)$ calculated with Eq. (5) were low-pass filtered using a cut-off frequency of 500 Hz to eliminate too rapid variations. Figs. 4 and 5 show the HHS of the first two IMFs for both LCs for the channels AE-1 and AE-2, respectively. As expected because of the higher load, the HHS for the signal in the LC N°2 contains higher amplitudes in each HHS. Taking into account the channel AE-1, the HHS of the first IMF (see Figs. 4(a) and 4(b)) is similar for both LCs. A variable frequency mode with frequencies approximately between 200 and 350 kHz is observed. However, for the second IMF (Figs. 4(c) and 4(d)) low-amplitude peaks of high frequency up to 230 kHz are revealed for the LC N°2. There are also present frequencies in the band between 120 and 160 kHz for both cases. Notice that the frequency peaks occur right before the maximal amplitudes of 300 mV shown in Fig. 3(b), so that in these signals only 7 frequency peaks are present. Similar behavior is also observable for the channel AE-2. In this case, the HHS of the first IMF (see Figs. 5(a) and 5(b)) have frequencies between 200 and 330 kHz for both LCs. Although for the LC N°2 some not well-defined peaks have frequencies up to 150 kHz. For the second IMF (see Figs. 5(c) and 5(d)), clearly defined peaks with frequency up to 190 kHz are revealed for the LC N°2. There are also present frequencies in the band between 110 and 150 kHz for both cases.
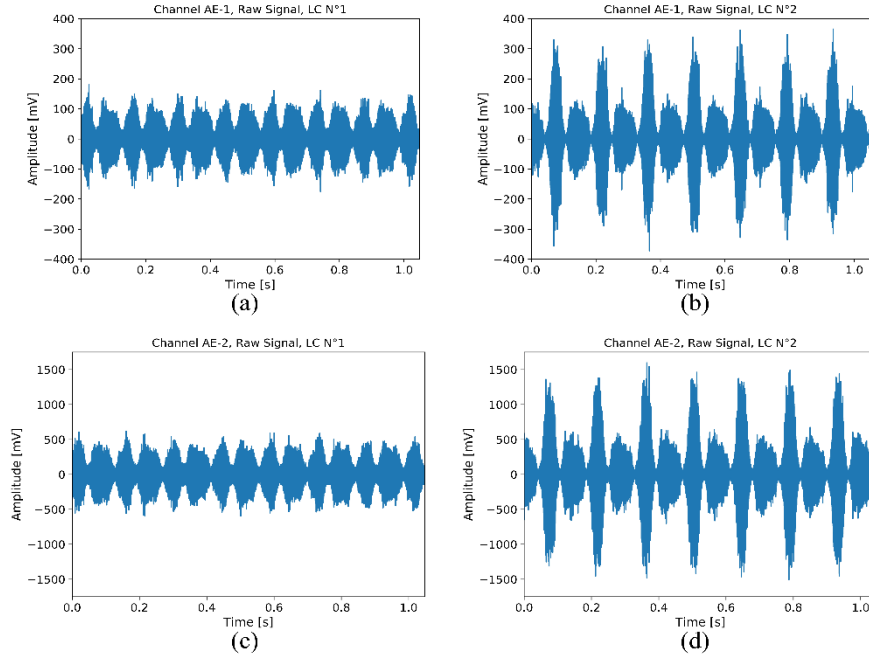
Fig. 3 AE signals of channel AE-1 for LCs N°1 (a) and N°2 (b), and for channel AE-2 for LCs N°1 (c) and N°2 (d)
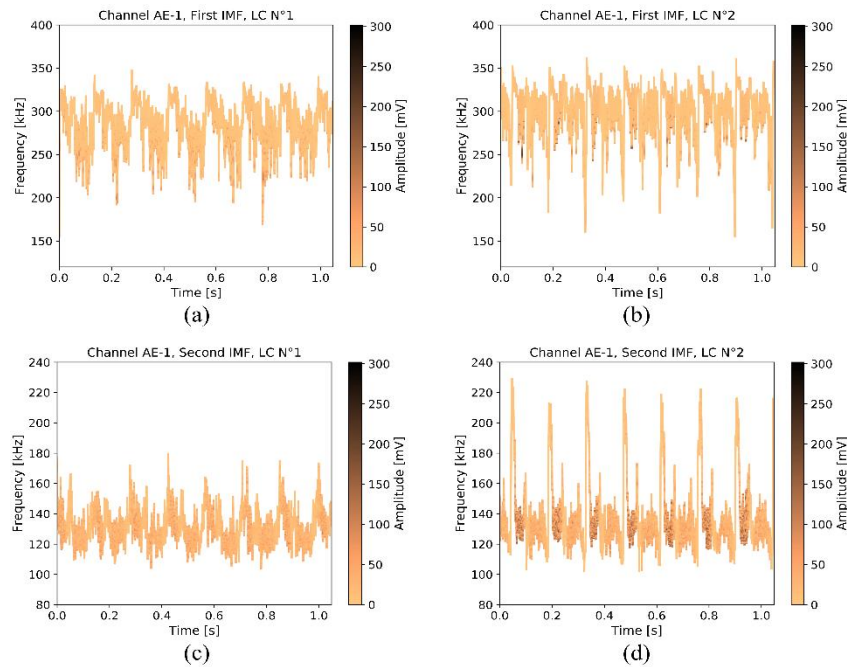

Fig. 4 HHS of the first IMF of channel AE-1 for LCs N°1 (a) and N°2 (b), and of the second IMF for LCs N°1 (c) and N°2 (d)
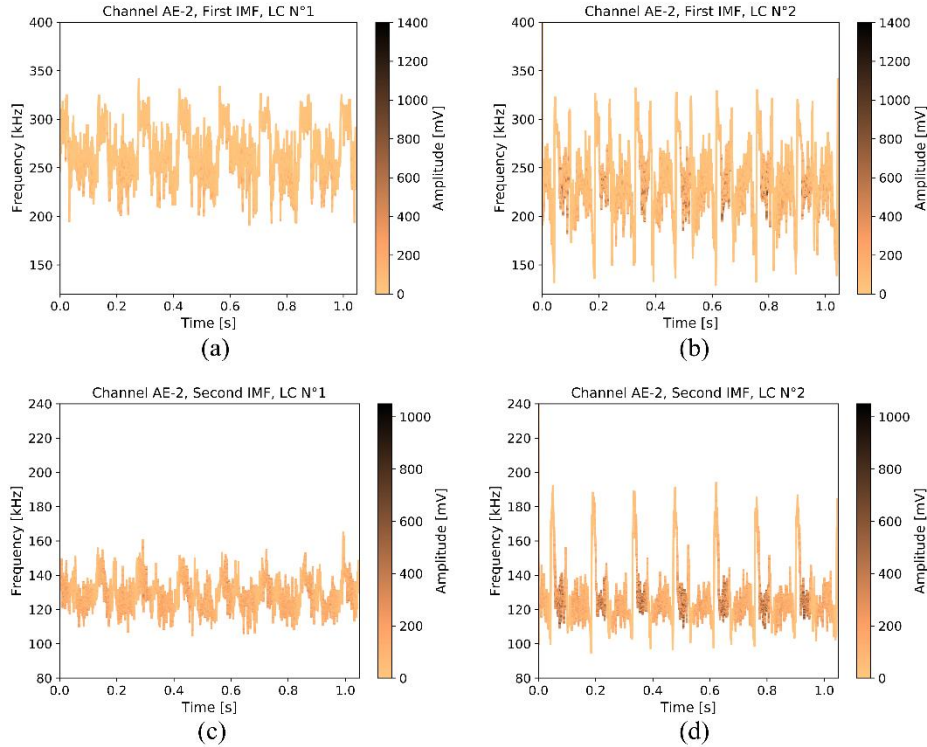
Fig. 5 HHS of the first IMF of channel AE-2 for LCs N°1 (a) and N°2 (b), and of the second IMF for LCs N°1 (c) and N°2 (d)

4.3 Evolution of frequency peaks

In this section the progression of the observed phenomenon is investigated. First, five approximately equally spaced instants along the duration of the LC N°2 were chosen, and segments of 1.048 s in every one of them were analyzed. In each of the segments the HHS was obtained following the same procedure of the results of section 4.2 considering the second IMF. Then, in every one of the frequency peaks the maximal frequency was determined and an average of the seven peaks within each segment was calculated. Fig. 6 shows the results of this procedure. As it can be seen, both channels have an increasing trend in the value of the frequency peaks.

In a further analysis, five instants along the duration of the LC N°1 were also chosen to investigate the evolution of the HHS during both LCs. The frequency range observed in the HHS of the second IMF were divided into four frequency bands and the energy of each band was calculated. For each point in the HHS the energy is the squared value of the instantaneous amplitude. Fig. 7 shows the energy evolution of each frequency band during the whole experiment. A logarithmic scale was used for visualization purposes. In the first half of the LC N°1 the energy is concentrated only below the 180 kHz, but in the second half energy in the frequency band 180-220 kHz for channel AE-1 (see Fig. 7(a)) appears. After the change of the LC, for the channel AE-1 the energy in the 180-220 kHz band increases and energy in the band 220-260 arises. For the channel AE-2, energy appears in the band 180-220 kHz only for the LC N°2 (see Fig. 7(b)).
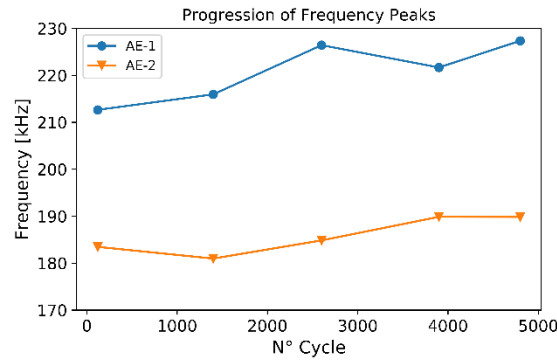
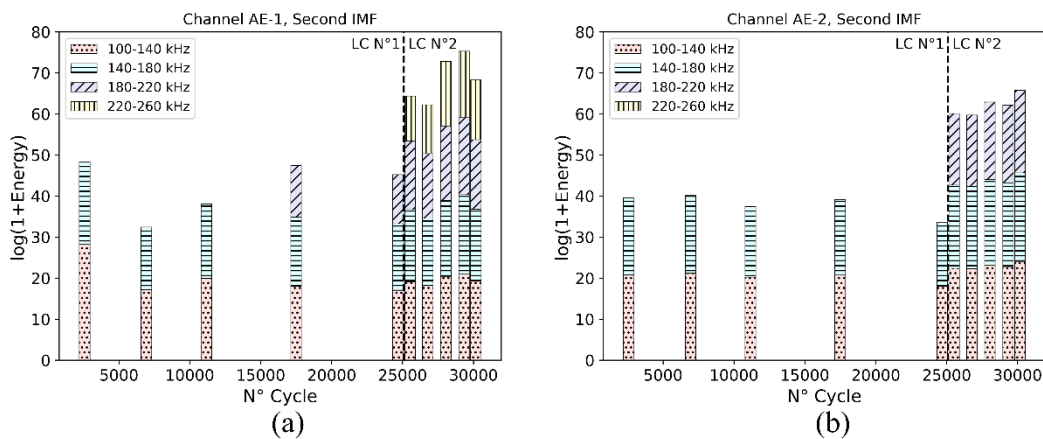Fig. 6 Frequency increase of the frequency peaks during LC N°2

Fig. 7 Energy evolution of frequency bands of the second IMF during the experiment for channels AE-1 (a) and AE-2 (b)

5. Analysis of results

For the AE signals in time-domain, the Fig. 3 shows waveforms with high amplitude modulation at 7 Hz. In the LC N°1 (see Figs. 3(a) and 3(c)) both conditions (maximal traction with 550 N and minimal traction with 450 N) produced a maximal AE amplitude of approximately 100 mV for the channel AE-1 and 500 mV for the channel AE-2. On the contrary, in the LC N°2 (see Figs. 3(b) and 3(d)) the maximal AE amplitude was almost tripled at the maximal traction for both channels, while it remains the same for the minimal traction. In the transition between maximal and minimal traction the signals reach an amplitude near zero. One hypothesis for this behavior is that the AE is mainly originated from impacts at the maximal and minimal traction instants of time, rather than a continuous emission depending on the traction force. Following this assumption, when the traction force was either 400, 450 or 550 kN the impacts produce a maximal amplitude of 100 mV for channel AE-1 and 500 mV for channel AE-2, but when the traction force was 600 kN the maximal amplitudes

were highly increased.

The signals with high modulation at 7 Hz made the finding of AE bursts impossible with traditional techniques such as amplitude thresholding (Hellier, 2003). However, when the HHS analysis was carried out, important differences between the two LCs were found. For the second IMF high-frequency peaks with low amplitude were discovered inside the background noise for both channels in the LC N°2 (see Figs. 4(d) and 5(d)). This behavior is a first sign of damage progression at the maximal traction point of LC N°2. This potential damage progression not only produced an amplitude increase in the AE signals as mentioned in the previous paragraph, but also the origination of frequency peaks buried in the continuous emission due to their low amplitude. These frequency peaks could only be revealed by the analysis of the instantaneous frequency using the HHS.

Previous studies have indicated the decrease of the average frequency of AE specific sources with the distance (Aggelis *et al*., 2012; Yu and Yang, 2009). In this work, the revealed frequency peaks for channel AE-1 reached frequencies up to 230 kHz (see Fig. 4(d)), but for channel AE-2 they suffered a frequency drop to 190 kHz (see Fig. 5(d)). Since the sensor AE-1 is significantly closer to the notch than the sensor AE-2, the frequency drop suggests that the frequency peaks were being generated from a specific source near sensor the AE-1. Therefore, this behavior is a second sign that the frequency peaks were probably originated from crack propagation at the position of the notch.

The analysis showed in Fig. 6 indicated that the generation of the frequency peaks were an on-going process, i.e. although the conditions of the LC N°2 were fixed, the frequency peaks increased their frequency as long as the experiment continued. The same deduction can be deducted from Fig. 7, in which it is observed that the AE energy increased in higher frequency bands in the second half of the LC N°1. Then, the energy increase in higher frequency bands was highly accentuated in the LC N°2. A similar behavior was found in the study from Kostryzhev *et al*. (2013) in fatigue tests of rail steel. They attributed the frequency peaks to brittle fracture and also observed a sustained increase in the average AE frequency after the crack on-set. Other studies from Li *et al.* (2009) and Marfo *et al.* (2013) in steel specimens have also indicated that during crack propagation the AE bursts increase their main frequency as the crack progresses. Therefore, the described behavior of frequency increase with accumulation of load cycles is a third sign that the frequency peaks found in the HHS are associated with damage progression.

6. Discussion

The work aimed to detect fatigue damage in its early stages in experiments carried out using a heavy-duty bolt. Such topic is of great relevance in the field of structural health monitoring, since an early damage detection gives maintenance engineers higher flexibility to adapt their maintenance schedules. The topic was approached by the use of AE sensors, which offer capacity to measure crack initiation and growth.

The results obtained from a fatigue testing experiment showed that the AE signals were highly influenced by impacts at the minimal and maximal traction instants of the load cycles. These impacts produced unwanted noise, which made the finding of AE bursts impracticable with traditional techniques to analyze AE signals. Therefore, advanced signal processing techniques that provide a higher time-frequency resolution were required. Within these methods, the HHS was tested and noticeable findings were obtained. As the damage began, frequency peaks of low amplitude appeared in the time-frequency representation of the IMFs of the sensor close the crack. This

frequency peaks were also visible for the sensor away from the crack, but with a frequency drop. Moreover, as the number of cycles cumulated the energy in higher frequency bands increased. These three signs can be attributed to the initiation of damage in the bolt, and therefore should be further investigated as damage detection features of AE signals.

Although this study shows the benefits of the HHS for analysis of AE signals during fatigue testing, more research is needed to validate the established remarks. In particular, the measurement of AE and analysis through the HHS should be performed during long-term fatigue testing, i.e. until the specimen reaches the failure. Only then the described behavior can be validated by monitoring its evolution together with the fault progression.

7. Conclusions

An experimental study on damage detection during fatigue testing using AE signals and the HHS as analysis tool was carried out. With the obtained results it is possible to establish the following conclusions:

- The waveforms of AE signals measured during fatigue testing have a shape of continuous emission with amplitude modulation rather than a constant amplitude with clearly visible transient AE bursts. This behavior was unaltered when conventional filters were applied.
- From the two LCs tested, at the maximal traction point of LC Nº2 the amplitude of the modulated waveform was highly increased and frequency peaks with low amplitude were revealed in the HHS of the second IMF. This finding could be associated with damage propagation in the specimen.
- The aforementioned frequency peaks had a higher frequency in the AE signals measured near the notch in comparison with the AE signals measured at the other end of the bolt. This frequency drop indicated that the peaks were generated near the notch or probably in it.
- The frequency of the peaks increased along the duration of the LC N°2. In addition, the AE energy increased in higher frequency bands not only in the LC N°2, but also since the second half of the LC N°1. This behavior suggests that the generation of frequency peaks was an on-going process attributed to crack growth rather than load change.

In this paper the findings of a study case were presented. In account of the probabilistic nature of fatigue and the multiple and unpredictable sources of AE, the results should be validated with measurements from different bolts and especially with experiments containing a higher number of load cycles, ideally until failure.

References

Aggelis, D.G., Shiotani, T., Papacharalampopoulos, A. and Polyzos, D. (2012), "The influence of propagation path on elastic waves as measured by acoustic emission parameters", *Struct. Health Monit.*, **11**(3), 359-366. https://doi.org/10.1177/1475921711419992.

Bhuiyan, M.Y., Bao, J., Poddar, B. and Giurgiutiu, V. (2018), "Toward identifying crack-length-related resonances in acoustic emission waveforms for structural health monitoring applications", *Struct. Health Monit.*, **17**(3), 577-585. https://doi.org/10.1177/1475921717707356.

Carlos, M.F. (2003), Heeding the warning sounds from materials, *ASTM Standardization News* **31**, 26-29.

Danyuk, A., Rastegaev, I., Pomponi, E., Linderov, M., Merson, D. and Vinogradov, A. (2017), "Improving of

acoustic emission signal detection for fatigue fracture monitoring", *Procedia Eng.*, **176**(2017), 284-290. https://doi.org/10.1016/j.proeng.2017.02.323.

Du, F. and Li, D. (2019), "Non-destructive evaluation and pattern recognition for SCRC columns using the AE technique", *Struct. Monit. Maint.*, **6**(3), 173-190. https://doi.org/10.12989/smm.2019.6.3.173.

Hamdi, S.E., Le Duff, A., Simon, L., Plantier, G., Sourice, A. and Feuilloy, M. (2013), "Acoustic emission pattern recognition approach based on Hilbert-Huang transform for structural health monitoring in polymer-composite materials", *Applied Acoustics* **74**(5), 746-757. https://doi.org/10.1016/j.apacoust.2012.11.018.

Han, Z., Luo, H., Cao, J. and Wang, H. (2011), "Acoustic emission during fatigue crack propagation in a micro-alloyed steel and welds", *Mater. Sci. Eng.: A* **528**(25-26), 7751-7756. https://doi.org/10.1016/j.msea.2011.06.065.

Hellier, C.J. (2003), *Handbook of Nondestructive Evaluation*. McGraw-Hill, New York, USA.

Huang, N., Shen, Z., Long, S., Wu, M., Shih, H., Zheng, Q., Yen, N., Tung, C. and Liu, H. (1998), "The empirical mode decomposition and the Hilbert spectrum for nonlinear and non-stationary time series analysis", *Proceedings of the Royal Society of London. Series A: Mathematical, Physical and Engineering Sciences* **454**, 903-995. https://doi.org/10.1098/rspa.1998.0193.

Huang, M., Jiang, L., Liaw, P.K., Brooks, C., Seeley, R. and Klarstrom, D. (1998), Using acoustic emission in fatigue and fracture materials research, *JOM-e: Research Summary* **50**.

Keshtgar, A. and Modarres, M. (2013), Acoustic emission-based fatigue crack growth prediction, *Proceedings Annual Reliability and Maintainability Symposium*, Orlando, USA, January. https://doi.org/10.1109/RAMS.2013.6517715.

Kostryzhev, A., Davis, C.L. and Roberts C. (2013), "Detection of crack growth in rail steel using acoustic emission", *Ironmaking & Steelmaking*, **40**(2), 98-102. https://doi.org/10.1179/1743281212Y.0000000051

Kratochvilova, V., Vlasic, F., Mazal, P. and Palousek, D. (2017), "Fatigue behaviour evaluation of additively and conventionally produced materials by acoustic emission method", *Procedia Structural Integrity* **5**(2017), 393-400. https://doi.org/10.1016/j.prostr.2017.07.187.

Li, L., Peng, Z. and Zhao, M. (2009), "In-situ monitoring of active crack in steel structure using acoustic emission technique", *Proceedings of the 2009 International Conference on Measuring Technology and Mechatronics Automation*, Zhangjiajie, China, April. https://doi.org/10.1109/ICMTMA.2009.384.

Li, H.N., Yi, T.H., Ren, L., Li, D.S. and Huo, L.S. (2014), "Reviews on innovations and applications in structural health monitoring for infrastructures", *Struct. Monit. Maint.*, **1**(1), 1-45. https://doi.org/10.12989/smm.2014.1.1.001.

Lu, C., Ding, P. and Chen, Z. (2011), "Time-frequency analysis of acoustic emission signals generated by tension damage in CFRP", *Procedia Eng.*, **23**(2011), 210-215. https://doi.org/10.1016/j.proeng.2011.11.2491.

Marfo, A., Chen, Z. and Li, J. (2013), "Acoustic emission analysis of fatigue crack growth in steel structures", *J. Civil Eng. Constr. Technol.*, **4**(7), 239-249. https://doi.org/10.5897/JCECT2013.0224.

Nair, A., Cai, C.S., Pan, F. and Kong, X. (2014), "Acoustic emission monitoring of damage progression in CFRP retrofitted RC beams", *Struct. Monit. Maint.*, **1**(1), 111-130. https://doi.org/10.12989/smm.2014.1.1.111.

Ono, K., Cho, H. and Takuma, M. (2005), "The origin of continuous emissions", *J. Acoust. Emission*, **23**(2005), 206-214.

Ruiz-Carcel, C., Hernani-Ros, E., Cao, Y. and Mba, D. (2014), "Use of spectral kurtosis for improving signal to noise ratio of acoustic emission signal from defective bearings", *J. Fail. Anal. Prevention*, **14**(3), 363-371. https://doi.org/10.1007/s11668-014-9805-7.

Siracusano, G., Lamonaca, F., Tomasello, R., Garesci, F., La Corte, A., Carni, D.L., Carpentieri, M., Grimaldi, D. and Finocchio, G. (2015), "A framework for the damage evaluation of acoustic emission signals through Hilbert-Huang transform", *Mech. Syst. Signal Pr.*, **75**(2016), 109-122. https://doi.org/10.1016/j.ymssp.2015.12.004

Stranghöner, N., Lorenz, C., Feldmann, M., Citarelli, S., Bleck, W., Münstermann, S. and Brinnel, V. (2018), „Sprödbruchverhalten hochfester Schrauben großer Abmessungen bei tiefen Temperaturen", *Stahlbau*

87(1), 17-29. https://doi.org/10.1002/stab.201810559

Vraetz, T., Boos, F.D., Röllinger, D., Bernet, C., Büschgens, C., Baltes, R. and Nienhaus, K. (2016), "Potentials and applications of the acoustic emission technology in mining and heavy machinery", *Proceedings of the 11ᵗʰ Aachener Kolloquium für Instandhaltung, Diagnose und Anlagenüberwachung*, Aachen, Germany, November.

WenQin, H., Ying, L., AiJun, G. and Yuan, F.G. (2016), "Damage modes recognition and Hilbert-Huang transform analyses of CFRP laminates utilizing acoustic emission technique", *Appl. Compos. Mater.*, **23**(2), 155-178. https://doi.org/10.1007/s10443-015-9454-3.

Yang, Z., Yu, Z., Xie, C. and Huang, Y. (2014), "Application of Hilbert-Huang transform to acoustic emission signal for burn feature extraction in surface grinding process", *Measurement*, **47**(2014), 14-21. http://dx.doi.org/10.1016/j.measurement.2013.08.036.

Yu, Y. and Yang, P. (2009), "Research of acoustic emission characteristics based on the signal parameters", *Proceedings of the International Conference on Information Engineering and Computer Science*, Wuhan, China, December. https://doi.org/10.1109/ICIECS.2009.5364817

Zhang, X., Wang, Y., Wang, K., Shen, Y. and Hu, H. (2017), "Rail crack detection based on the adaptive noise cancellation method of EMD at high speed", *Proceedings of the IEEE International Instrumentation and Measurement Technology Conference*, Turin, Italy, May. https://doi.org/10.1109/I2MTC.2017.7969662

Zhao, L., Kang, L. and Yao, S. (2018), "Research and application of acoustic emission signal processing technology", *IEEE Access*, **7**(2018), 984-993. https://doi.org/10.1109/ACCESS.2018.2886095.

JK